Models for the Adsorption and Self-Assembly of Ethanol and 1-Decanethiol on Au(111) Surfaces. A Comparative Study by Computer Simulation

FILOMENA F. M. FREITAS, RUI P. S. FARTARIA, FERNANDO M. S. SILVA FERNANDES

Molecular Simulation Group, CCMM, Department of Chemistry and Biochemistry, Faculty of Sciences, University of Lisboa, Campo Grande, Bloco C8, 1749-016 Lisboa, Portugal

Received 16 January 2009; accepted 10 March 2009
Published online 3 June 2009 in Wiley InterScience (www.interscience.wiley.com).
DOI 10.1002/qua.22254

ABSTRACT: Results from computer simulations, based on different models to study theadsorption and self-assembly of the ethanol and 1-decanethiol on gold surfaces, Au(111), are presented. Canonical ensemble Monte Carlo simulations were performed at 298 K using two different force fields. One from DFT calculations, where the gold electrode has an explicit structure (corrugated electrode), and the other representing an electrode, in which the structure is taken into account on an average way (flat electrode). The behavior of the ethanol adsorption on gold surfaces, with and without the 1-decanethiol presence, is analyzed. The introduction of molecular flexibility is also discussed. The relative surface density for the ethanol oxygen, adsorbed on gold, and the density profiles, in different conditions, show that the structure of the surface has a fundamental role on the way the adsorption takes place, not only on the preferential adsorption sites of the surface but also on the ethanol distribution over the electrodes. Potentials of mean force have also been calculated for the two surface models, giving the free energy barriers to the 1-decanethiol crossing of the solvent adsorption layers. The average tilt angle, obtained with a single

Correspondence to: F. F. M. Freitas; e-mail address: fffreitas@fc.ul.pt

Rui P. S. Fartaria is currently at Department of Chemical and Process Engineering, University of Strathclyde, Glasgow, G1 IXJ, Scotland.

Contract grant sponsor: Fundação para a Ciência e a Tecnologia (FCT, Portugal).

thiol molecule in the simulation box, presents the values: $\sim 26^\circ$ for the rigid molecule model and $74^\circ \pm 18^\circ$ for the flexible one. These differences are analyzed. Int J Quantum Chem 110: 293–306, 2010

Key words: ethanol; alkylthiol; gold electrode; absorption; self-assembly

1. Introduction

Potential energy surfaces (PES) are crucial to study reactive and nonreactive chemical systems by computer simulation. To investigate the mechanisms involved in the adsorption and self-assembly of solvated molecules on noble-metal electrodes, the PES should describe the interactions between the different molecular species present in the liquid phase, including the contribution of their intramolecular forces, as well as the interactions of those species with the electrodes, in terms of distances and orientation angles.

Self-assembly provides an attractive method for the preparation of organized, stable, and versatile monolayers onto metallic surfaces, with a defined composition and a close-packed structure. The self-assembly process consists of physi- and chemisorption of molecules followed by their spontaneous organization. The resulting films are called self-assembled monolayers (SAMs) [1–3]. The research in this field started in the 1980s, and its applications range from biosensing to corrosion prevention and lubrication.

SAMs can be prepared using different types of molecules and substrates. The process needs a molecule that is normally an alkane chain, with $\geq$10 methylene units, and a head group with strong preferential adsorption to the substrate. Thiol (S-H) head groups and Au(111) substrates are usually used because of the well-known affinity between sulfur and gold. The thiol molecules adsorb readily from a solution onto gold, creating a dense monolayer with the tail chain pointing outward from the electrode surface. By using thiol molecules with different tail chains, the resulting chemical surface functionality can be varied within wide limits. It is also possible to functionalize the tail chains through chemical reactions after the SAMs are formed.

The probe of SAMs by surface analytical methods, such as infrared spectroscopy [4, 5], ellipsometry [6–8], and other techniques, has shown that alkane chains with a length of 12 or more methylene units form well-ordered and dense monolayers on Au(111) surfaces [9].

Most of the simulations carried out hitherto have started from monolayers already assembled, considering the interaction thiolate-metal, and mainly focusing on structural, dynamical, and interfacial properties [10–15]. Other studies have given particular attention to the nature of the bond between the thiolate and the Au(111) surface [16–19]. Simulations with different models have predicted tilt angles in the range of 20–30°, in good agreement with experiment [20]. Ab initio calculations of the chemisorbed state (thiolate-gold bonding) have concluded that the fcc surface-site of Au(111) is the preferential one for physi- and chemisorption [17].

Our general objective is to carry out a detailed study starting from the adsorbate, dispersed into the solvent, following its approach to the electrode, the physisorption and, finally, the reaction between the thiol head and the metal.

In this article, we review our previous results and report about new ones [21], concerned with the self-assembly of 1-decanethiol (from a dilute solution in ethanol) on Au(111) surfaces, pursuing our preliminary studies on such heterogeneous systems [22, 23]. Monte Carlo simulations based on DFT calculations for the ethanol–gold interactions are presented, in the context of a comparative analysis between a gold surface with an explicit structure [corrugated electrode (CE)] and a gold surface where the structure is taken into account on an average way [flat electrode (FE)]. The behavior of ethanol adsorbed on those gold surfaces, with and without the 1-decanethiol presence, is also analyzed. The surface relative density for the ethanol oxygen, adsorbed on gold, and the density profiles, in different conditions, show that the structure of the surface has a fundamental role on the way the adsorption takes place, not only on the preferential adsorption sites of the surface but also on the ethanol distribution over the electrodes. The potentials of mean force have also been calculated, for the two surface models, giving the free energy barriers to the 1-decanethiol crossing of the solvent adsorption layers.

An outline of the molecular interactions used in the simulations is given in the next section. Section 3 contains some simulation details. Section 4 reports and discusses the results obtained with

different models. Finally, Section 5 presents concluding remarks.

2. Molecular Interactions

The following molecular interaction models for ethanol–ethanol, ethanol–Au(111), ethanol–thiol–Au(111), and intramolecular degrees of freedom have been used. Full details are described elsewhere [21–23].

2.1. LIQUID-PHASE INTERACTIONS

The liquid-phase force fields, for rigid molecules (RM), were modeled using OPLS potentials [24, 25], described by a site–site potential ($U_{i,j}$) with Lennard–Jones (LJ) and coulombic contributions according to

$$U_{i,j} = \sum_{\alpha\in i}\sum_{\beta\in i}\frac{A_{\alpha,\beta}}{r_{\alpha,\beta}^{12}} - \frac{B_{\alpha,\beta}}{r_{\alpha,\beta}^{6}} + \frac{q_\alpha q_\beta}{r_{\alpha,\beta}}, \quad (1)$$

where A and B are the LJ parameters obtained from the combination rules of Berthelot and Lorentz, q is the partial charges on the sites and, r is the distance between sites.

For flexible molecules (FM), in addition to the previous site–site potential, we considered torsional motions about C–O bonds in ethanol and C–S bonds in thiol. Other dihedral angles were also included for thiol. The torsional potentials of Jorgensen [24, 25] for ethanol and of Hautman and Klein [10] for thiol were described by the general form

$$V_t(\phi) = V_0 + \frac{1}{2}V_1(1+\cos(\phi)) + \frac{1}{2}V_2(1-\cos(2\phi)) + \frac{1}{2}V_3(1+\cos(3\phi)), \quad (2)$$

where ϕ is the appropriate dihedral angle.

The bending motions were taken into account through the harmonic potential [10]

$$V_b(\theta_{ijk}) = \frac{1}{2}k_{ijk}^{\theta}\left(\theta_{ijk} - \theta_{ijk}^{0}\right)^2 \quad (3)$$

where θ is the appropriate bending angle defined by atoms i, j, and k.

2.2. ELECTRODE-MOLECULE INTERACTIONS

For the simulations of ethanol and thiol with a gold FE, we adopted the 12-3 potential, derived from the LJ potential, as described by Hautman and Klein [10] and Fartaria et al. [22]:

$$U(z) = \frac{C_{12}}{(r_z - r_{z_0})^{12}} - \frac{C_3}{(r_z - r_{z_0})^3} \quad (4)$$

where U is the potential energy,$C_n \propto \sqrt{\epsilon\sigma^n}$, r_{z_0} is the distance between each molecule site and the electrode. The C_{12} and C_3 parameters for the various sites are presented in Refs. [10, 22].

Regarding the ethanol–Au(111) interactions, the potential was parametrized on the basis of the ethanol oxygen–Au energy obtained either from preliminary DFT calculations (designated by O_{ab} parametrization) or from other two approximations (designated by O_{strong} and O_{weak} [22]). Most of the results referred to in this article, for the FE model, were obtained by the O_{ab} parametrization.

Another refined model has been developed by extensive DFT calculations considering a Au(111) CE [23].

The theory level to calculate the ethanol–Au(111) interaction energy was the hybrid B3LYP method [26, 27] with the LanL1MB basis set [28] applied to the gold atoms and the 6-31G basis set [29] for the H, C, and O atoms. The calculations were performed using the Gaussian 98 package [30].

A cluster of 14 Au atoms, to represent the gold surface and one ethanol molecule in the equilibrium gas-phase configuration with optimized geometry, was used to model the ethanol–Au(111) PES. This size was chosen, after testing clusters of different sizes, with a compromise between the consistency of the interaction energy and the computation time.

To probe the ethanol–Au(111) interactions, three sites of the gold surface were chosen as shown in Figure 1: the TOP site, where the O atom of the ethanol approaches the surface over a Au atom of the first layer; the hcp site named Hollow1 (H1), and the fcc site named Hollow2 (H2), where the O atom approaches the surface in the direction of the center of a triangle formed by three Au atoms of the first layer. The triangle of site H1 has a Au atom of the second layer at the center [23].

The ethanol–$Au(111)_{14}$ cluster interaction energy as a function of the distance and orientation, relatively to the gold cluster surface, is defined as

$$U_{\text{ethanol-Au(111)}_{14}}(r,\alpha,\beta) = U_{\text{Au(111)}_{14}+\text{ethanol}}(r,\alpha,\beta) - U_{\text{Au(111)}_{14}} - U_{\text{ethanol}}, \quad (5)$$

where $U_{\text{Au(111)}_{14}+\text{ethanol}}$ is the energy of the system composed by the ethanol molecule and the cluster;

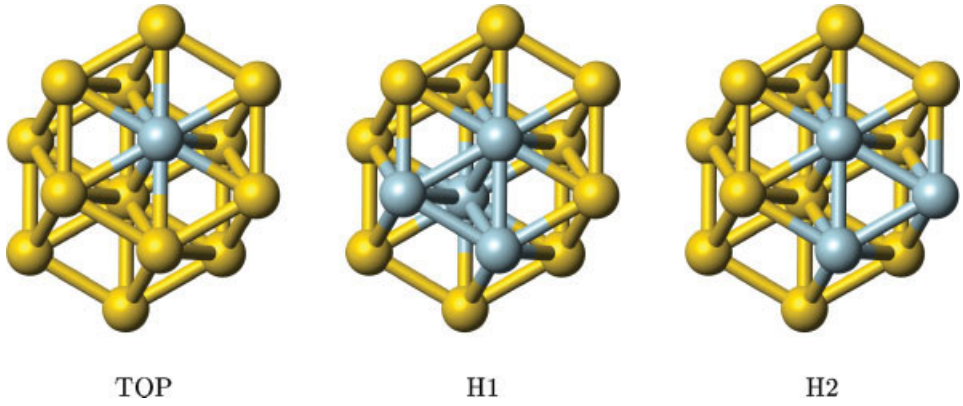

FIGURE 1. Gold sites (top, hollow1, and hollow2) chosen for modeling the ethanol–Au(111) surface interactions. [Color figure can be viewed in the online issue, which is available at www.interscience.wiley.com.]

$U_{\mathrm{Au(111)_{14}}}$ and U_{ethanol} are the energies of the isolated cluster and ethanol molecule, respectively; r is the distance from the ethanol oxygen atom to the plane of the firstlayer of the Au(111) surface; α is the angle between the O–H bond and the normal to the surface; and β is the angle between the H–O–C plane and the H–O−(normal to the surface) plane. The orientations for the ethanol molecule were selected to span a wide range of situations. For each orientation, several values of r (about 30), spanning the interval 0–10 Å, have been chosen, and the $U_{\mathrm{ethanol\text{-}Au(111)_{14}}}$ was evaluated.

The following analytical function was fitted to the afore mentioned DFT results:

$$\begin{aligned} &U_{\mathrm{EtOH\text{-}Au}} \\ &= U_{\mathrm{H}}(r_{\mathrm{H\text{-}Au}}) + (1 + B_0 \cos(\theta/\mathrm{rad})^{20}/r^3_{\mathrm{O\text{-}Au}}) \cdot U_{\mathrm{O}}(r_{\mathrm{O\text{-}Au}}) \\ &\quad + U_{\mathrm{CH_2}}(r_{\mathrm{CH_2\text{-}Au}}) + U_{\mathrm{CH_3}}(r_{\mathrm{CH_3\text{-}Au}}) + V(r_{\mathrm{O\text{-}Au}}, \theta, \phi) \end{aligned} \tag{6}$$

where

$$\begin{aligned} U_i(r_{i-\mathrm{Au}}) &= A_{0,i} \exp[A_{1,i}(r_{i-\mathrm{Au}} + A_{2,i})] \\ &\quad - A_{3,i} \exp[A_{4,i}(r_{i-\mathrm{Au}} + A_{5,i})] \end{aligned} \tag{7}$$

is the site–site interaction energy and

$$\begin{aligned} &V(r_{O-\mathrm{Au}}, \theta, \phi) \\ &\quad = C_0 \sin(\theta/\mathrm{rad})^6 \cdot \exp[(r \sin(\theta/\mathrm{rad}) - C_1)^2/C_2] \\ &\cdot [C_3 - C_4 \cos(3(\phi/\mathrm{rad} - C_5)) + C_6 \cos(6(\phi/\mathrm{rad} - C_5))] \end{aligned} \tag{8}$$

is the contribution due to the surface symmetry around a TOP side. The cosine term with exponent 20, in Eq. (6) can be expressed in other forms (e.g., $\exp(-10x^2)$). The details and fitting parameters can be seen elsewhere [23]. The interaction energy between the ethanol molecule and the surface is calculated as the sum of $U_{\mathrm{EtOH\text{-}Au}}$ over all the Au atoms in the surface.

Finally, for the thiol–Au(111) interactions, we have not yet a full DFT force field in terms of the thiol distance to the CE and the respective orientations. Therefore, in a first approximation, we considered that the thiol interacted with a FE.

It should be mentioned that the representation of metallic surfaces by cluster models has been a common approximation to minimize the heavy computational requirements. We have commented on that elsewhere [23, 31]. Yet, nowadays, accurate periodic DFT methods can be implemented in relatively low-cost computer networks. We will consider them in future applications to surface models.

2.3. SOFT WALL - MOLECULE INTERACTIONS

These interactions are only repulsive and acted on the center of mass of the ethanol and thiol molecules. Thus, the molecules in contact with the surface can rotate independently of it. They were modeled by the truncated and shifted LJ potential

$$\begin{cases} u^{\mathrm{LJ}}(r) - u^{\mathrm{LJ}}(r_{\min}) & r \le r_{\min} \\ 0 & r > r_{\min} \end{cases} \tag{9}$$

where $r_{\min}$ is the value of r at the minimum of the LJ potential curve.

3. Computational Details

NVT-Monte Carlo calculations have been performed at potential of zero charge (pzc) conditions,

some of them using the configurational-bias technique. The simulation box (37.5 Å × 39.9 Å base area and 65.8 Å height) contained 980 ethanol molecules, or 977 ethanol molecules and one 1-decanethiol molecule, between two distinct surfaces parallel to the xy plane: one representing a simple soft-wall and the other a gold electrode. In the corrugated model, the electrode had 416 gold atoms, distributed in two layers, according to the structure of the Au (111) surface. The dimensions of the box were chosen to match the ethanol density at 298 K and 1 atm (0.7873 g cm^{-3}). Periodic boundary conditions were only applied in the x and y directions.

The interaction between the soft-wall and ethanol or thiol was only applied to the mass center of the molecules, allowing the rotation of the molecules independently of that wall, even when they were near to it. This strategy was adopted to make the surface effects as short ranged as possible.

The LJ interactions for the liquid-phase molecules were truncated at half of the box side length. The respective coulombic interactions were taken into account either by the minimum image convention without truncation or by Ewald's sum.

Equilibration runs with 2×10^4 MC cycles were followed by production runs with 2×10^5 cycles. The effects of the introduction of one 1-decanethiol molecule in the interface were analyzed from production runs with 3×10^4 cycles.

4. Results and Discussion

4.1. COMPARISON OF THE MODELS FOR THE ETHANOL–Au(111) INTERFACE

To analyze the effects of introducing corrugation in the gold electrodes as well as intramolecular degrees of freedom in the ethanol molecules, relatively to the simpler model with FE and RM, we have calculated, for each ethanol molecule site (H, O, CH_2, and CH_3; note that the molecule is described by an united atom model), the density profiles (Fig. 2) and the bidimensional profiles of the relative superficial density for the molecules of the first adsorption layer (Fig. 4 and Fig. 5).

Figure 2 shows the density profiles of the ethanol sites for the models with a FE (with RM or FM) and with a CE (with RM or FM).

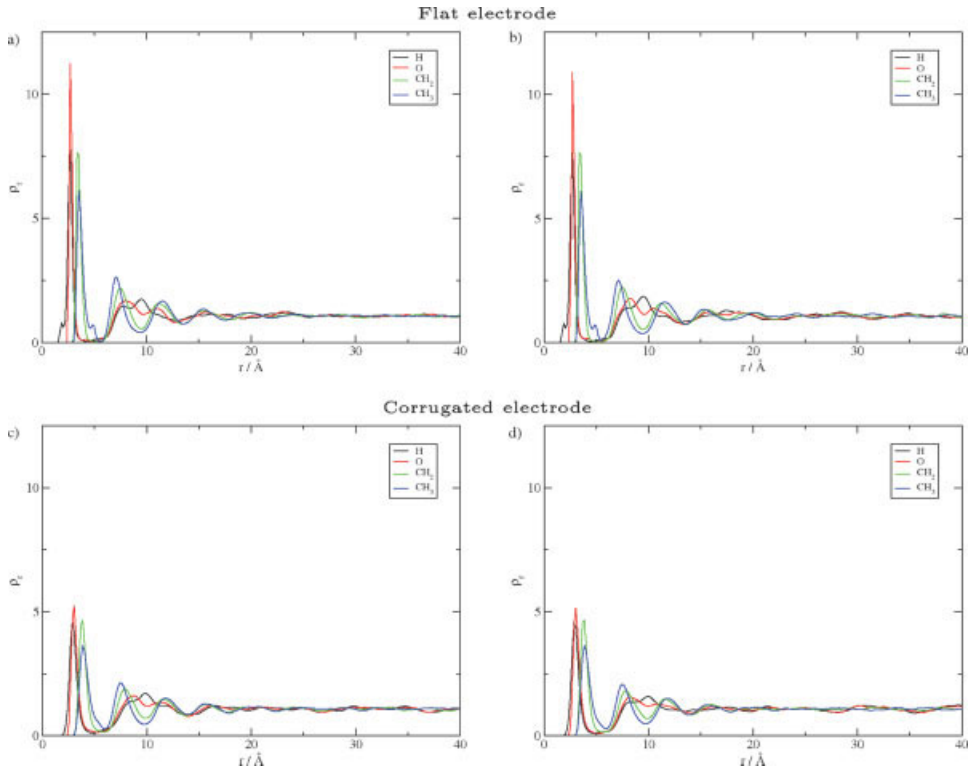

FIGURE 2. Density profiles of the ethanol for the flat electrode (a) with rigid molecules and (b) with flexible molecules and for the corrugated electrode (c) with rigid molecules and (d) with flexible molecules. [Color figure can be viewed in the online issue, which is available at www.interscience.wiley.com.]

TABLE I

Location of the density profiles peaks and adsorption layers (Fig. 2) for flat (FE) and corrugated (CE) electrodes (values in Å).

			With rigid molecules				With flexible molecules			
	Layer	Site	Peak	Layer loc.	Thickness	Molec. N.	Peak	Layer loc.	Thickness	Molec. N.
FE	1st	H	2.7; 2.0				2.7;1.9			
		O	2.7(or 8)	1.3–5.6	4.3	67	2.7	1.3–5.5	4.2	67
		CH_2	3.4(or 5)			(66 ± 1)	3.4			(66 ± 1)
		CH_3	3.5(6);4.9				3.5;4.9			
	2nd	H	7.7				7.9			
		O	8.1	5.6–9.6	4.0	66	8.2	5.5–9.5	4.0	66
		CH_2	7.5				7.5			
		CH_3	7.1				7.1			
	3rd	H	9.5;11.0				9.5;11.5			
		O	11.0	9.6–13.3	3.7	63	10.5	9.5–13.4	3.9	63
		CH_2	11.2				11.1			
		CH_3	11.5				11.6			
CE	1st	H	2.9				2.8			
		O	3.0	1.6–5.5	3.9	60	3.0	1.6–5.7	4.1	61
		CH_2	3.8			(59 ± 2)	3.8			(59 ± 2)
		CH_3	3.9				3.9			
	2nd	H	8.5				8.2			
		O	8.7	5.5–10.0	4.5	68	8.3	5.7–9.9	4.2	66
		CH_2	7.9				7.8			
		CH_3	7.5				7.5			
	3rd	H	9.8;11.8				10.0			
		O	11.5	10.0–14.0	4.0	67	11.0	9.9–13.8	3.9	64
		CH_2	11.6				11.5			
		CH_3	11.8				11.8			

The number of molecules (Molec. N.) also included.

The identification of the main peaks and the location of the adsorption layers of the density profiles of the Figure 2 are shown in Table I. The number of ethanol molecules in each adsorption layer, also included in the table, was calculated by integrating the density profiles of the interaction centers O and CH_3 by

$$n(Z_f) = \frac{N}{Z} \int_0^{Z_f} g(z)\, dz \qquad (10)$$

where N is the total number of molecules in the system, Z is the distance between the electrodes, and $g(z)$ is the relative density as a function of the distance to the electrode, z. The Table I also includes, in italic, the average number of the adsorbed molecules in the first adsorption layer.

The density profiles for the FE with RM, Figure 2, show the hydrogen peak at ~2.7 Å with a smaller one at ~2.0 Å, the oxygen peak at ~2.8 Å, the CH_2 peak at ~3.5 Å, and the strongest CH_3 peak at ~3.6 Å with a minor one at ~4.9 Å. This means that almost all the ethanol molecules are oriented, on average, with the plane of the molecule perpendicular to the electrode and the O–H bond almost parallel to the surface. The H and CH_3 smaller peaks, in the first layer, are possibly correlated showing that a small portion of these molecules is more vertically orientated toward the electrode, as we have discussed in Ref. [22]. The second layer is localized at ~7.5 Å with molecular orientations correlated to those of the first layer. For FM and FE, we can conclude from the Table I that the characteristics are the same as with RM. The adsorption layers are basically in the same position. However, only in the case of FM the electrode influence extends, smoothly, behind 20 Å. The peaks distribution in the first layer, with {O, H} and $\{CH_2, CH_3\}$ separated by ~0.8 Å, is in accordance with an average orientation of ethanol molecules in which the O–H bond is practically parallel to the surface and forming with the molecule plane an angle

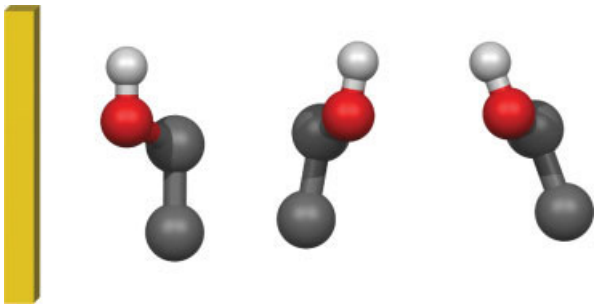

FIGURE 3. General orientations of ethanol molecules. From left to the right: first, second, and third layers. [Color figure can be viewed in the online issue, which is available at www.interscience.wiley.com.]

of ~45°. Observing the peaks distribution of the second and third layers, we can conclude that the sites CH_2 and CH_3 from the second are turned to the first, whereas the same sites from the third layer are turned to the bulk of the solution. Thus, the peaks O and H do the linking between these two layers as we can see in Figure 3, where the general orientations of ethanol molecules in first three adsorption layers are schematically represented. This observation, strengthened by the greater intensity of H peak of the third layer, strongly suggests the formation of hydrogen bonds between these two layers, and that the interaction between first and second layers is made by hydrophobic groups of the ethanol molecules. Another important detail, as it was already referred in Ref. [22], are the short peaks at ~2.0 Å for H, and at ~4.9 Å for CH_3, of the first layer. They indicate the existence of some deviations from the main orientation in these layer, with the molecules in a position nearer the normal to the surface [22].

From the density profiles of Figure 2 for the CE, we can conclude that the structure of the ethanol–Au(111) interface, regarding the molecules orientations relatively to surface, presents essentially the same behavior, with a similar main distribution, displayed in Figure 3. However, with this new force field, in which the ethanol–Au(111) interactions are calculated explicitly for each gold atom in the surface, it is observed a considerable reduction of the peaks intensity of the first adsorption layer. This is associated to a reduction, from ~67 to ~60 (Table I), in the number of ethanol molecules in the first adsorption layer. This effect is a pure consequence of the different ethanol–Au(111) interaction models, as it occurs with both RM and FM.

Figures 4 and 5 show the relative superficial density for the sites of the ethanol molecule in the first adsorption layer. We defined the relative superficial density of a molecule site as the average of the local superficial density of the site, divided by the average of the superficial density of the adsorbed molecules.

From the profiles, we can take some qualitative information about the molecules distribution and their mobility on the surface. Thus, in the system with the FE and RM (4, on the left side), we can see the existence of four molecule sets and, also, chain structures with several ethanol molecules. Around

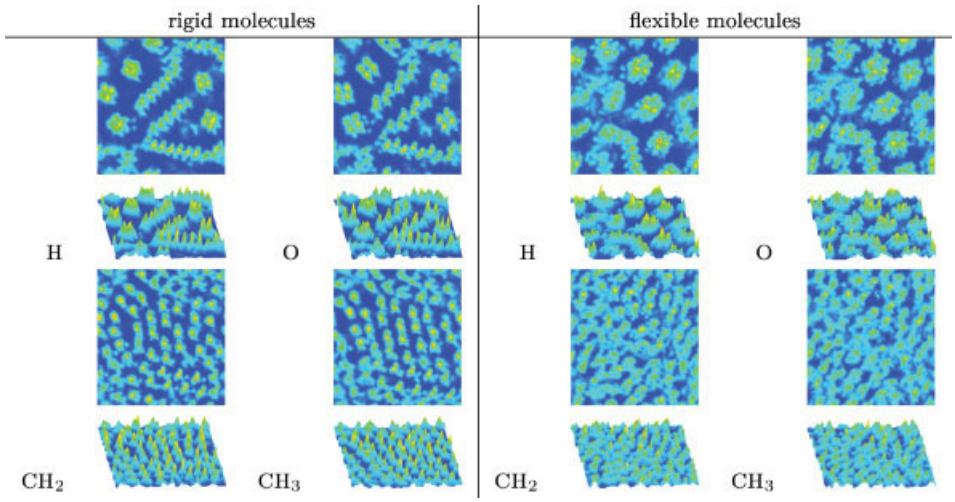

FIGURE 4. Relative superficial density for the sites of ethanol molecules in first adsorption layer: Au flat electrode and rigid or flexible ethanol molecules. [Color figure can be viewed in the online issue, which is available at www.interscience.wiley.com.]

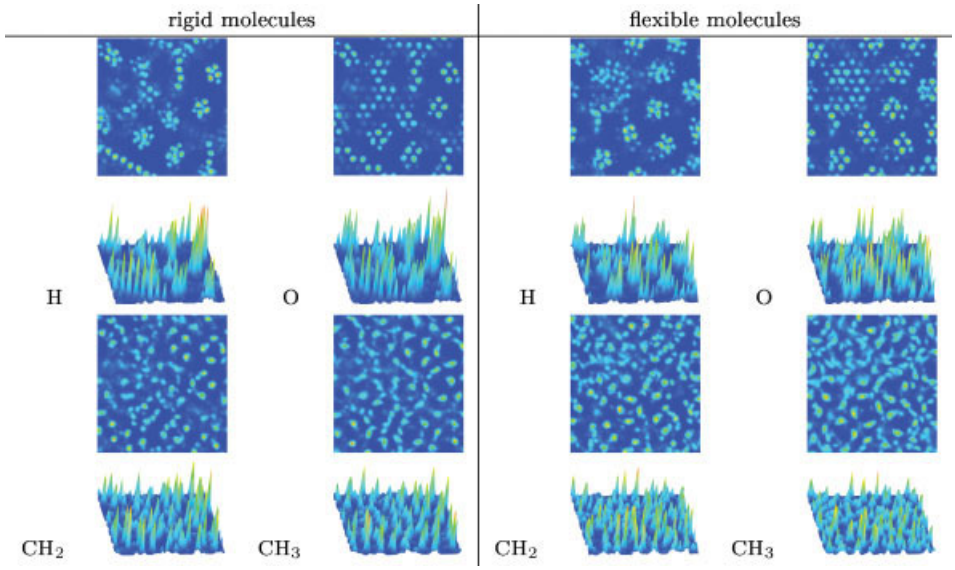

FIGURE 5. Relative superficial density for the sites of ethanol molecules in first adsorption layer: Au(111) corrugate electrode and rigid or flexible ethanol molecules. [Color figure can be viewed in the online issue, which is available at www.interscience.wiley.com.]

the four molecules set, we can observe, in the H and O profiles, the nonexistence of another sites around them. Taking into account the orientations obtained from the density profiles, that emptiness should result from stereochemical impediments of the CH_2 and CH_3 sites. As for the profiles for the CH_2 and CH_3 sites, we observe a more uniform packing with larger peaks, suggesting a greater mobility for these sites. The introduction of flexibility in the ethanol molecules, keeping the FE (Fig. 4, on the right), shows a greater tendency for the formation of the four ethanol molecule sets and less chains. The general enlargement of peaks for the four sites, relatively to the ones on the left side, suggests that the molecules have greater mobility as an effect of introducing intramolecular degrees of freedom.

Figure 5 displays the relative superficial densities for the sites of the ethanol molecules in the first adsorption layer on the Au(111) CE, with RM or FM.

Changing from the ethanol–gold 12-3 potential to the new force field, referred to in section 2.2 and proposed elsewhere [23], introduced substantial modifications in the superficial distribution and mobility of the ethanol molecules. According to what was discussed previously, the influence of this change in the "vertical" distribution of the molecules is not very important, the only consequence being a decreasing on molecules number of the first adsorption layer. From the profiles of Figure 5, on the left, we can conclude that the ethanol molecules, adsorb on surface, through the O atom, preferentially on surface TOP sites [23] as we can see in Figure 6. We can also observe the formation of some sets of four molecules and some tendency to chain formations. However, the sharpening of peaks for the H and O sites reveals a shorter "horizontal" mobility of the adsorbed molecules. Figure 5, on the right, presents profiles corresponding to the introduction of intramolecular freedom degrees, where it can be seen the disappearing of the chains and a greater incidence of molecular sets formation. These profiles indicate a more diffuse peaks distribution, suggesting a greater mobility for the molecules.

In the cases presented so far, the calculation of the Coulomb interactions was made by the minimum image approximation without cut off. More realistic calculations were done using Ewald summation for two dimensions [32]. The results are shown in Figures 7 and 8.

Table II contains the locations of the density profiles peaks and adsorption layers, and the average number of molecules in each adsorption layer. Comparing the density profiles of Figures 2(b) and 7, we can see that they are rather similar. However, from the profiles in Figures 5, for the FM, and 8, we can detect some small differences. The clusters of four and five molecules, in the calculations with Ewald's sum, are slightly reduced, or their structures are not so well defined. We also can verify the formation of a short chain with four or five ethanol molecules.

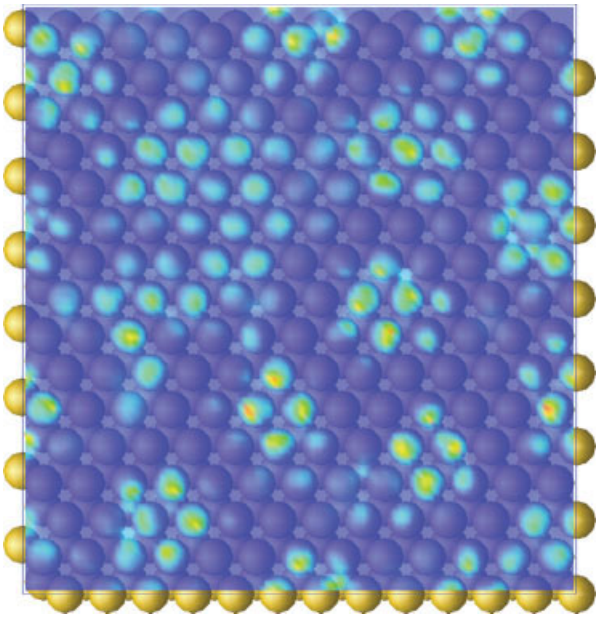

FIGURE 6. Projection of the superficial density of the ethanol-O sites, in the first layer, over the Au(111) surface. [Color figure can be viewed in the online issue, which is available at www.interscience.wiley.com.]

4.2. ADSORPTION OF 1-DECANETHIOL ON THE ETHANOL–Au(111) INTERFACE. POTENTIAL OF MEAN FORCE

In our previous study of the adsorption of 1-decanethiol, solvated by ethanol, on Au(111) surfaces, [22] the molecules were considered rigid and the electrode flat.

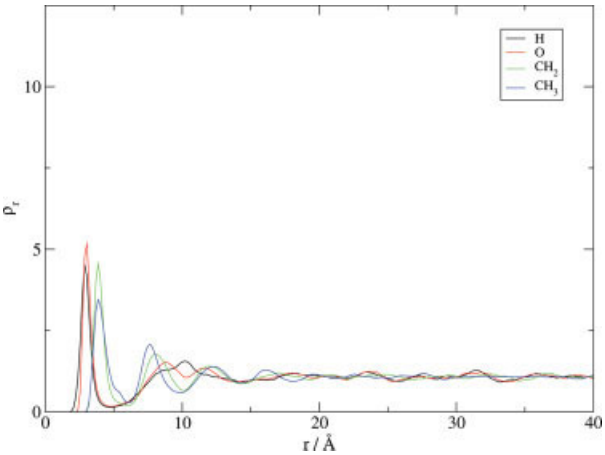

FIGURE 7. Density profiles for the corrugated electrode with flexible ethanol molecules and long range interactions calculated by Ewald's sum. [Color figure can be viewed in the online issue, which is available at www.interscience.wiley.com.]

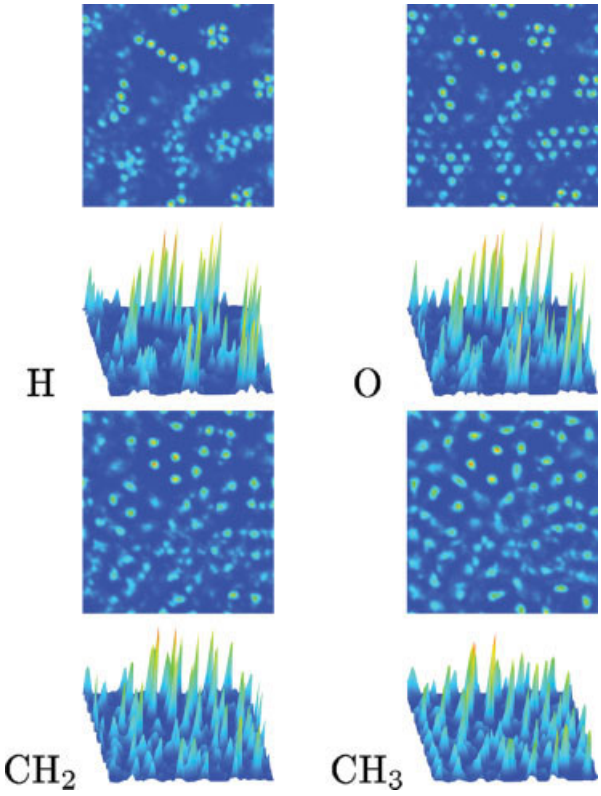

FIGURE 8. Relative superficial density for the ethanol sites, in the first layer: corrugated electrode, flexible molecules, and long-range interactions calculated by Ewald's sum. [Color figure can be viewed in the online issue, which is available at www.interscience.wiley.com.]

TABLE II

Locations of density profiles peaks and adsorption layers of Figure 7 (values in Å).

Layer	Site	Peak	Layer loc.	Thickness	Molec. N.
1st	H	2.9			
	O	3.0	1.5–5.5	4.0	60
	CH_2	3.8			58 ± 2
	CH_3	3.9			
2nd	H	8.7			
	O	8.8	5.5–10.3	4.8	70
	CH_2	8.0			
	CH_3	7.6			
3rd	H	10.2			
	O	11.5	10.3–14.3	4.0	65
	CH_2	11.9			
	CH_3	12.3			

The number of molecules (Molec. N.) also included.

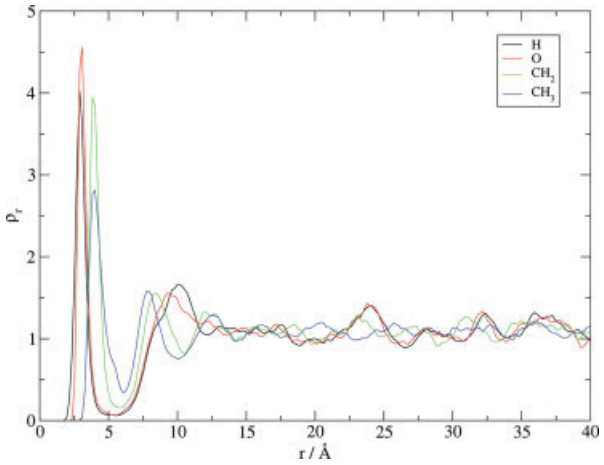

FIGURE 9. Density profiles of the ethanol in a system with a 1-decanethiol molecule adsorbed on the ethanol–Au(111) interface. [Color figure can be viewed in the online issue, which is available at www.interscience.wiley.com.]

Here, we present new simulation results from a refined model in which we take into account the intramolecular degrees of freedom for the ethanol and 1-decanethiol molecules (applying to the thiol molecules the Monte Carlo configurational-bias method [33]) as well as the explicit corrugation of the electrode for the ethanol–Au(111) interactions. The respective interaction potentials have been referred to above.

Figure 9 presents the density profile for the ethanol molecules versus the distance to the electrode. Figure 10 shows superficial density profiles for the first adsorption layer, as a projection on the electrode surface.

Figure 11 presents a snapshot of a first adsorption layer configuration of ethanol molecules, including a 1-decanethiol molecule adsorbed on the electrode surface.

Comparing the density profiles of Figures 9 with the ones in Figure 7, for the same model but without the 1-decanethiol molecule, we observe that the peak heights of the first adsorption layer are less intense indicating, as expected, a decreasing of the number of ethanol molecules in the first adsorption layer, because of the introduction of one thiol molecule. In fact, the average number of ethanol molecules in the first adsorption layer is now 46 ± 2. The number of ethanol molecules delocalized by the thiol molecule is $\sim$10. This number should be related not only with the space occupied by the thiol molecule but also with its impact in the structure of the ethanol–Au(111) interface. This is shown in Figures 10 and 11. In the superficial density projection the region occupied by the thiol molecule is identified by the more intense blue area corresponding to the minimum value of the ethanol-O sites density. In the snapshot of Figure 11 the thiol molecule (with hydrophobic chain in cyan) is almost in a horizontal position relatively to the surface.

The average tilt angle of the thiol molecule (defined as the angle between the normal to the surface and the line that passes through the sulfur atom and the mass center of the last four chain sites (MCL4), counted from the sulfur atom) is $74^\circ \pm 18^\circ$. Thus, the configuration presented in the Figure 11 is just an instantaneous one. Indeed, as we shall see ahead, the tilt angle changes along the simulation.

The relative orientation of the ethanol molecules that surround the thiol molecule should also be mentioned. All the molecules surrounding the aliphatic chain are oriented so that the CH_2 and CH_3 sites are turned to it. On the other hand, the O and H sites of ethanol are turned to the S and H sites of thiol, suggesting the formation of hydrogen bonding. It is also observed the formation of some clusters of four and five molecules, in a ring form, in accordance to the superficial density profiles, with the O and H sites

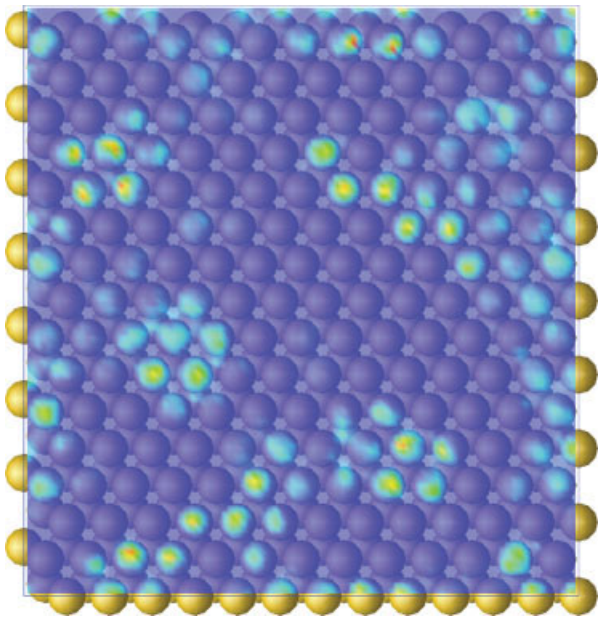

FIGURE 10. Projection of superficial density profile of O from the first adsorption layer, with a 1-decanethiol adsorbed on the ethanol–gold interface. [Color figure can be viewed in the online issue, which is available at www.interscience.wiley.com.]

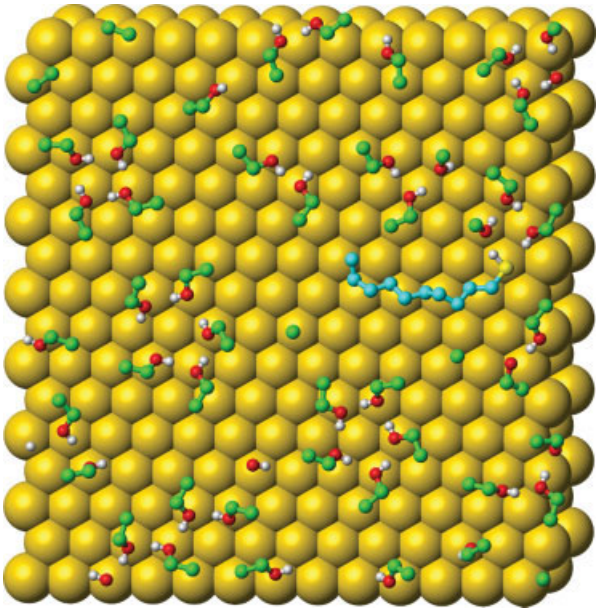

FIGURE 11. Snapshot of a first adsorption layer configuration including a 1-decanethiol molecule adsorbed on the electrode surface. [Color figure can be viewed in the online issue, which is available at www.interscience.wiley.com.]

turned toward the inside of the ring, with a probable formation of hydrogen bonding, and two CH_2 and CH_3 sites directed toward the outside. In the area above the aliphatic chain, it is evident the formation of a chain of five or six molecules of ethanol, also observable in the superficial density profile.

The approach of the 1-decanethiol molecule to the electrode surface was followed through the calculation of the potential of mean force (PMF) [34–38], similarly to our work on the simpler model [22]. The solvent contribution to PMF, that is, the Helmholtz free energy corresponding to the solvent–thiol interaction, indicates the effect of the solvent on the approach of the thiol molecule to the electrode. Simulations were carried out, in the range of 2.7–13.9 Å, along the normal to the surface. Additionally to the PMF, the average length and tilt angle of the 1-decanethiol molecule were also calculated. The results are presented in Figures 12, 13 and 14, respectively.

Comparing the PMF graphic of the Figure 12 with the ones previously reported by us [22], it seems that, in this model, the effect of the solvent is similar to the one of the O_{strong} model. The change in free energy indicates, as expected, the increasing difficulty of 1-decanethiol in penetrating the adsorption layers

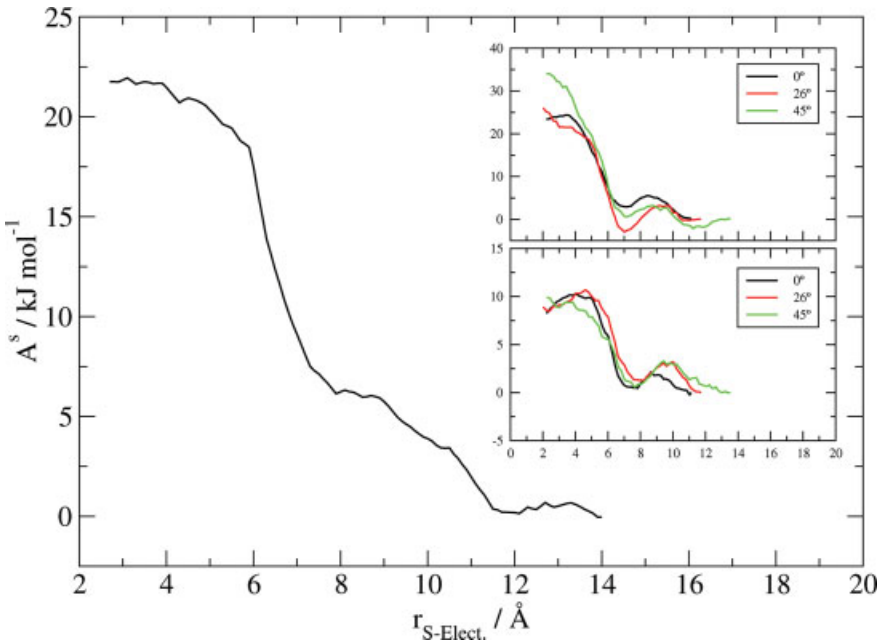

FIGURE 12. Solvent PMF of the more accurate model (with flexible molecules). Insets: Solvent PMF of the O_{strong} (up) and the O_{weak} (down) models for three orientations of rigid thiol molecules (with flat electrode; adapted from [22]). $r_{S\text{-}Elect.}$ is the distance from the sulfur atom to the electrode surface. [Color figure can be viewed in the online issue, which is available at www.interscience.wiley.com.]

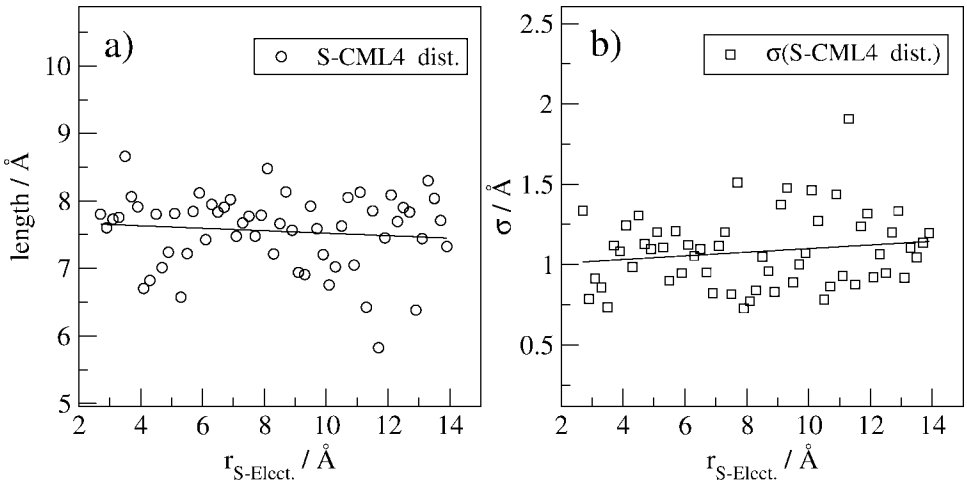

FIGURE 13. (a) Average length of the thiol molecule in function of the distance to the electrode. (b) Standard deviations of the values presented in (a).

of the solvent. However, the O_{strong} model shows a noticeable repulsion decrease of the thiol molecule, when passing from the second to the first layer. In the present refined model, such repulsion decrease is not apparent, but a quasi-continuous increase of the free energy with a small step at the crossing of the layers is observed instead. This effect can be attributed to the fact that in the O_{strong} model the approach is made with a RM in a fixed orientation, whereas in this model the molecule changes into a great variety of configurations.

Figures 13 and 14 also reveal some aspects of the 1-decanethiol molecule as it approaches the electrode surface.

The dispersion and the standard deviation of the molecule length (S-CML4) and the tilt angle indicate the degree of the variety of configurations that the thiol molecule can assume in these conditions. It would be necessary to have a much larger statistics, in the simulations, to obtain a sounder information on these properties. However, some general conclusions may be drawn from a linear regression of the presented values. Thus, Figure 13 shows that the length of 1-decanethiol molecule tends to increase with the approach to the electrode. Moreover, the standard deviation of this property tends to decrease leading to the conclusion that the length tends to stabilize. In Figure 14 [graphic (a)], the tilt angle

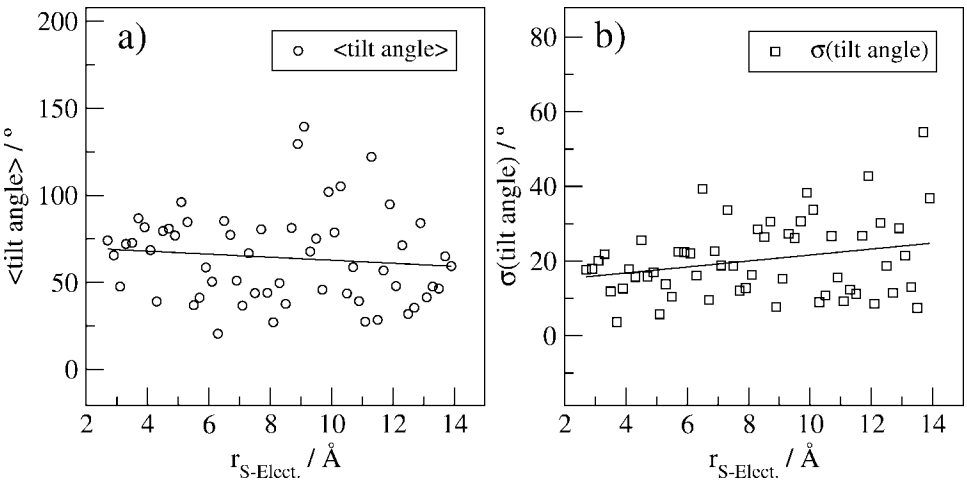

FIGURE 14. (a) Average tilt angle of the thiol molecule in function of the distance to the electrode. (b) Standard deviations of the values presented in (a).

of the thiol molecule increases as it approaches the electrode. The decrease of the standard deviation of this angle [graphic (b)] indicates, in turn, that the value of the angle is more stable when the molecule is nearer to the electrode. The tilt angle value of 1-decanethiol molecule, in this model, is $74^\circ \pm 18^\circ$ as already referred to above. This value differs significantly from the one obtained with the RM models, $\sim 26^\circ$. It is to point out that the present values are for the adsorption of an unique thiol molecule. The tilt angle is, in this in case, much influenced by the type of interactions between the alkylic chain and the solvent molecules, which are, obviously, different from the interactions between the chains in a self-assembled layer, where the value of the tilt angle, determined experimentally and computationally, is $\sim 30^\circ$ [10, 16, 20].

As the latter model is more accurate, we deduce that the 26° angle is an artefact of the rigid models, being the $\sim 74^\circ$ value more realistic for a single thiol molecule in the system. The thiol molecule seems to adsorb oscillating relatively to the electrode surface in a somewhat elongated form.

5. Conclusions

These results allow us to conclude that the main effects of increasing the modeling accuracy of the ethanol molecules and of the molecule-surface interactions are as folows: the "vertical" organization of the solvent layers (along the normal to the surface) is, in general, little sensitive to the introduced modifications, suggesting that such organization depends more on the characteristics of the system itself than on the details of the interactions along the distance to the electrode surface; the flexibility introduced in the ethanol molecules originates their greater mobility at the interface; and the corrugation of the surface as well as the force field across it, though not having much influence on the "vertical" distribution of the adsorption layers, change, significantly, the "horizontal" distribution of the adsorbed molecules. Presumably, it is this interface modification that affects strongly the ethanol molecules packing and to which we should attribute the decrease in the number of molecules located at the first adsorption layer.

The structure of the electrode has noticeable effects on the distribution of the adsorbed molecules, as seen in the relative surface densities. These indicate that: (i) on flat surfaces the ethanol molecules (rigid or flexible) form some chains and clusters with four or five molecules; and (ii) on corrugated surfaces the chains occur less frequently, which might be related to a reduced mobility of the molecules due to their preferential adsorption on the top sites.

The potential of mean force has the same behavior in all models. The solvent offers resistance to the thiol adsorption that grows as the adsorption layers are crossed.

The length of the flexible thiol molecule has a remarkable change, increasing and stabilizing when it approaches the electrode, as indicated by the respective standard deviation.

The number of ethanol molecules adsorbed on gold electrode decreases when the structured model is used.

The thiol average tilt angle has different values depending on the use of RM ($\sim 26^\circ$) or flexible ones ($74^\circ \pm 18^\circ$). The latter value was obtained with a single thiol molecule in the simulation box. In the corrugated surface model, the tilt angle increases and stabilizes as the molecule approaches the surface. Calculations with a greater number of thiol molecules in the simulation box are in progress. We expect that, in this case, the simultaneous interactions between various thiol and ethanol molecules, using the more accurate model, shall approach the experimental average tilt angle ($\sim 30^\circ$).

This work needs to be extended not only in what concerns the number of thiol molecules in the models but also regarding a much finer screening, by DFT, of the different gold interaction sites and ethanol orientations. Indeed, before a full simulation analysis, and its comparison with experiment, can be performed, it is necessary to obtain DFT results for gold sites other than the Top, H1, and H2 to increase the accuracy of the PES. In this context, we have recently applied neural networks techniques to assist the mapping of multidimensional PES from DFT calculations [39, 40].

References

1. Nuzzo, R. G.; Fusco, F. A.; Allara, D. L. J Am Chem Soc 1987, 109, 2358.
2. Swalen, J. D.; Allara, D. L.; Andrade, J. D.; Chandros, E. A.; Garoff, S.; Israelachvili, J.; Mccarty, T. J.; Murray, R.; Pease, R. F.; Rabolt, J. F.; Wynne, K. J.; Yu, H. Langmuir 1987, 3, 932.
3. Viana, A. S.; Jones, A. H.; Abrantes, L. M.; Kalaji, M. J Electroanal Chem 2001, 500, 290.
4. Nuzzo, R. G.; Dubois, L. H.; Allara, D. L. J Am Chem Soc 1990, 112, 558.
5. Nuzzo, R. G.; Korcnic, E. M.; Dubois, L. H. J Chem Phys 1990, 93, 767.

6. Bain, C. D.; Troughton, E. B.; Tao, Y. T.; Evall, J.; Whitesides, G. M.; Nuzzo, R. G. J Am Chem Soc 1989, 111, 321.
7. Whitesides, G. M.; Labinis, P. E. Langmuir 1990, 6, 87.
8. Evans, S. D.; Urankar, E.; Ulman, A.; Ferris, N. J Am Chem Soc 1991, 113, 4121.
9. Sukhinin, Y. V. J Exp Theor Phys 1998, 87, 115.
10. Hautman, J.; Klein, M. L. J Chem Phys 1989, 91, 4994.
11. Siepmann, J. J.; McDonald, I. R. Mol Phys 1993, 79, 457.
12. Sadreev, A. F.; Sukhinin, Y. V. Phys Rev B 1996, 54, 54.
13. Pertizin, A. J.; Grunze, M. Langmuir 2000, 16, 8829.
14. Jiang, S. Mol Phys 2002, 100, 2261.
15. Gronbech-Jensen, N.; Paikh, A. N.; Beardmore, K. M.; Desai, R. C. Langmuir 2003, 19, 1474.
16. Sellers, H.; Ulman, A.; Shnidman, Y.; Eilers, J. E. J Am Chem Soc 1993, 115, 9389.
17. Yourdshahyan, Y.; Zhang, H. K.; Rappe, A. M. Phys Rev B 2001, 63, 081405.
18. Vargas, M. C.; Giannozzi, P.; Selloni, A.; Scoles, G. J Phys Chem B 2001, 105, 9509.
19. Yourdshahyan, Y.; Rappe, A. M. J Chem Phys 2002, 117, 825.
20. Porter, M. D.; Bright, T. B.; Allara, D. L.; Chidsey, C. E. D. J Am Chem Soc 1987, 109, 3559.
21. Fartaria, R. P. S. Fullerenes and Self-Assembly Study by Computer Simulation, PhD Thesis, Faculty of Sciences of University of Lisboa, 2007.
22. Fartaria, R. P. S.; Freitas, F. F. M.; Fernandes, F. M. S. S. J Electroanal Chem 2005, 574, 321.
23. Fartaria, R. P. S.; Freitas, F. F. M.; Fernandes, F. M. S. S. Int J Quantum Chem 2007, 107, 2169.
24. Jorgensen, W. J Phys Chem 1986, 90, 1276.
25. Jorgensen, W. J Phys Chem 1986, 90, 6379.
26. Becke, A. D. J Chem Phys, 1993, 98, 5648.
27. Becke, A. D. J Chem Phys 1993, 98, 1372.
28. Hay, P. J.; Wadt, W. R. J Chem Phys 1985, 82, 270.
29. Hehre, W. J.; Ditchfield, R.; Pople, J. A. J Chem Phys 1972, 56, 2257.
30. Frisch, M. J.; Trucks, G. W.; Schlegel, H. B.; Scuseria, G. E.; Robb, M. A.; Cheeseman, J. R.; Zakrzewski, V. G.; Montgomery, J. A.; Stratmann, R. E.; Burant, J. C.; Dapprich, S.; Millam, J. M.; Daniels, A. D.; Kudin, K. N.; Strain, M. C.; Farkas, O.; Tomasi, J.; Barone, V.; Cossi, M.; Cammi, R.; Mennucci, B.; Pomelli, C.; Adamo, C.; Clifford, S.; Ochterski, J.; Petersson, G. A.; Ayala, P. Y.; Cui, Q.; Morokuma, K.; Malick, D. K.; Rabuck, A. D.; Raghavachari, K.; Foresman, J. B.; Cioslowski, J.; Ortiz, J. V.; Stefanov, B. B.; Liu, G.; Liashenko, A.; Piskorz, P.; Komaromi, I.; Gomperts, R.; Martin, R. L.; Fox, D. J.; Keith, T.; Al-Laham, M. A.; Peng, C. Y.; Nanayakkara, A.; Gonzalez, C.; Challacombe, M.; Gill, P. M. W.; Johnson, B. G.; Chen, W.; Wong, M. W.; Andres, J. L.; Head-Gordon, M.; Replogle, E. S.; Pople, J. A. Gaussian 98, Gaussian Inc.: Pittsburgh, PA, 1998.
31. Neves, R. S.; Motheo, A. J.; Fartaria, R. P. S.; Fernandes, F. M. S. S. J Electroanal Chem 2007, 609, 140.
32. Yeh, I.-C.; Berkowitz, M. L. J Chem Phys 1999, 111, 3155.
33. Frenkel, D.; Smit, B. Understanding Molecular Simulations: From Algorithms to Applications, 2nd ed.; Academic Press: San Diego, 2002.
34. Reynolds, C. A.; King, P. M.; Richards, W. G. Mol Phys 1992, 76, 251.
35. Spohr E. Chem Phys Lett 1993, 207, 214.
36. Spohr E. Acta Chem Scand 1995, 49, 189.
37. Mezei, M.; Beveridge, D. L. Ann NY Acad Sci 1986, 482, 1.
38. Ignaczak, A.; Gomes, J. A. N. F.; Romanowski, S. J Electroanal Chem Interfacial Electrochem 1998, 450, 175.
39. Latino, D. A. R. S.; Fartaria, R. P. S.; Freitas, F. F. M.; Aires de Sousa, J.; Silva Fernandes, F. M. S. J Electroanal Chem 2008, 624, 109.
40. Latino, D. A. R. S.; Fartaria, R. P. S.; Freitas, F. F. M.; Aires de Sousa, J.; Silva Fernandes, F. M. S. Int J Quantum Chem 2009, 109 (in press).